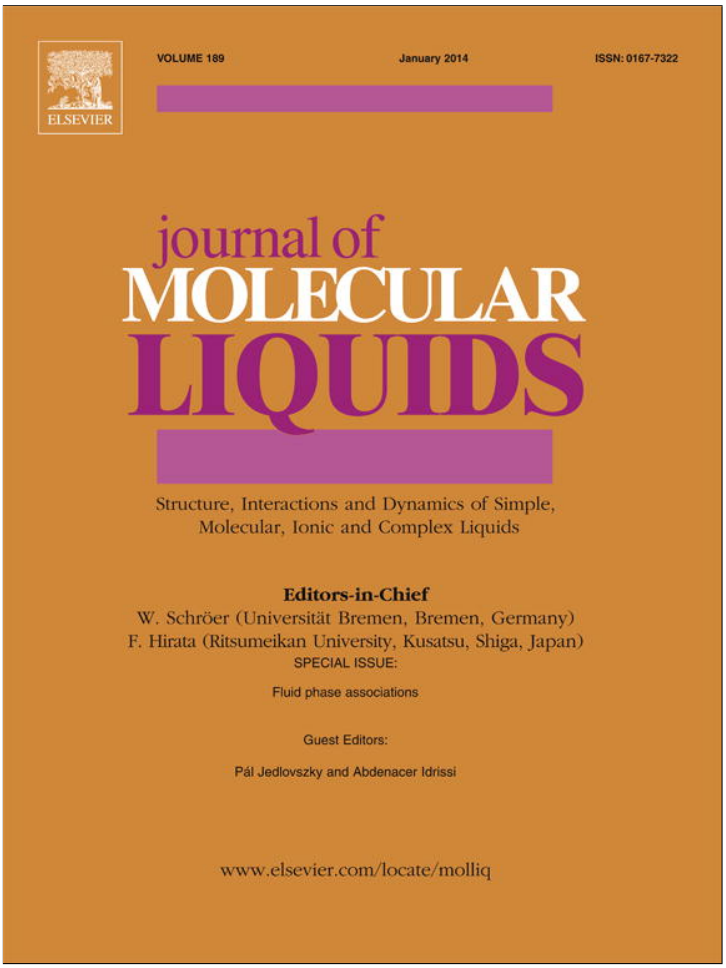

Journal of Molecular Liquids 189 (2014) 100–112

Contents lists available at ScienceDirect

Journal of Molecular Liquids

journal homepage: www.elsevier.com/locate/molliq

Selective transport through a model calcium channel studied by Local Equilibrium Monte Carlo simulations coupled to the Nernst–Planck equation

Dezső Boda [a,*], Róbert Kovács [a], Dirk Gillespie [b], Tamás Kristóf [a]

[a] Department of Physical Chemistry, University of Pannonia, P. O. Box 158, H-8201 Veszprém, Hungary
[b] Department of Molecular Biophysics and Physiology, Rush University Medical Center, Chicago, IL, USA

ARTICLE INFO

Available online 23 April 2013

Keywords:
Transport
Monte Carlo
Nernst–Planck
Ion channel

ABSTRACT

We have recently introduced the Local Equilibrium Monte Carlo (LEMC) technique (Boda, Gillespie, J. Chem. Theor. Comput. 8 (2012) 824-829) in which a non-equilibrium system is divided into small volume elements and separate Grand Canonical Monte Carlo simulations are performed for each using a local intensive parameter, which, as soon as local equilibrium is assumed, can be identified with the local electrochemical potential. The simulation provides the concentration profiles of the steady-state diffuse system, where ions are transported through a membrane from one bulk compartment to the other. The dynamics of the ions is described with the Nernst–Planck (NP) transport equation. The NP equation is coupled to the LEMC simulations via an iteration procedure that ensures that conservation of mass (the continuity equation) is satisfied. We apply the method to a simple calcium channel model and demonstrate its efficiency. The computer experiments are inspired by real electrophysiological experiments for the Ryanodine Receptor calcium channel. The diffusion coefficients in the channel are fitted to results of Dynamic Monte Carlo simulations.

1. Introduction

Biological and technological phenomena occur in non-equilibrium conditions where intensive thermodynamic variables (temperature, pressure, chemical potential) are different in different subspaces of the system with matter and/or energy being transported from one compartment to the other. An important case is when molecules or ions diffuse through a membrane from the compartment on one side of the membrane to the compartment on the other side. The membrane can be a porous matrix as in the case of zeolites [1–3] or a non-penetrable layer with embedded pores (artificial nanopores etched into plastic foil [4–6] or biological ion channels [7,8]) that make the transport possible. In the most important cases, these pores discriminate between particles allowing the selective transport of various components, thus giving the membrane a special function in the respective biological or technological situations. Ion channels, in addition, can be gated, namely, they open or close as a result of an appropriate signal. A recent study [9] indicates that gating is possible in nanopores too by bubble formation mediated by an external electric field.

Ion channels span the cell membrane, thus making the transport of various physiologically relevant ions possible through the membrane selectively. Calcium (Ca) channels, in particular, make the passage of Ca^{2+} ions possible with a much larger probability than that of monovalent ions such as Na^{+} or K^{+} even if they are present in the bath in much smaller quantity than the monovalent ions. The physiological importance of these channels cannot be overemphasized. The L-type Ca channel in the membrane of muscle cells, for example, lets Ca^{2+} ions into the cell when an action potential arrives [10]. Ryanodine Receptor (RyR) Ca channels, on the other hand, are located in the membrane of the sarcoplasmic reticulum. When they are triggered to open (by, for example, the Ca^{2+} ions provided by the L-type Ca channel), they release a large amount of Ca^{2+} ions into the muscle cell, thus initiating muscle contraction.

The selectivity properties of these channels are an essential part of their functions in this chain of information-processing at the end of which a muscle is contracted. To understand selectivity mechanisms of such tiny pores, we need modeling. The model should contain all the relevant information available for the respective channel. The model, in turn, is studied with a statistical mechanical method. Computer simulations have become the most important method in the last decades thanks to the constant increase in the speed of computers. Theories [11–18], however, remain as a useful alternative to simulations. Our purpose in this paper is to apply and test a newly proposed simulation method to study permeation and selectivity properties of Ca channels.

When we talk about selectivity, we can look at the same thing from two points of view [19]. Selectivity can be studied as a selective binding (also termed binding affinity) that describes the probabilities with which the competing ions are adsorbed to a certain binding site. In the case of channels, this binding site is the selectivity filter, which is the bottleneck of the pore, where ions are attracted with electrostatic and van der Waals forces (no chemical bonds are involved). Selective binding can be characterized by the average numbers of the respective

* Corresponding author. Tel.: +36 88624325.
E-mail address: boda@almos.vein.hu (D. Boda).

0167-7322/$ – see front matter © 2013 Elsevier B.V. All rights reserved.
http://dx.doi.org/10.1016/j.molliq.2013.03.015

ions in the selectivity filter (occupancies). This phenomenon has been studied by Grand Canonical Monte Carlo (GCMC) simulations [20–27], Density Functional Theory (DFT) [13,14,28–30], and other theories [11,12,15,17].

In practice and in electrophysiological measurements, however, the really important quantity is the current carried by the respective ions. We can define dynamical selectivity as the ratio of fluxes of the competing ions. In experiments, current–voltage relations are obtained for various electrolyte compositions on the two sides of the membrane. Drawing conclusions from such data to selectivity properties is not obvious because experiments provide the net current carried by both ions.

Qualitative conclusions are sometimes straightforward as in the case of the L-type Ca channel, where adding Ca^{2+} to 30 mM NaCl blocks the current when [Ca^{2+}] is micromolar [10,31,32]. This fact implies that Ca^{2+} ions bind preferentially to the selectivity filter even if they are present in 1 μM quantity in the bath. The effect of this selective binding on transport properties is relatively easy to decipher because selectivity is so strong and the effect is so characteristic. In the general case, however, we need modeling and calculations to separate the fluxes carried by the competing ions.

Simulation of transport phenomena is much more difficult than that of equilibrium phenomena. The obvious tool for simulating a non-equilibrium system is molecular dynamics (MD) for an explicit-solvent model and Langevin dynamics (LD) or Brownian dynamics (BD) for an implicit-solvent model [33–35]. MD solves Newton's equations of motion, computes trajectories, and provides time averages. LD and BD include a frictional and a stochastic term describing interactions with water molecules. LD and BD, therefore, solve a system of stochastic differential equations, while MD solves a system of partial differential equations (PDE). What is common in them is that they both provide macroscopic properties from a purely mechanic description.

Dynamic Monte Carlo (DMC) is an alternative method, where MC displacements are used instead of time steps. DMC does not generate trajectories in time as MD or LD do, but it mimics them in a way that an average over them gives the same answer for the mean-square displacement that time averages over MD or LD trajectories give. DMC proved to be especially useful in simulating dynamical selectivity [19], namely, the ratio of the fluxes for various ionic species, because DMC does not include an absolute measure of time; it only ensures proportionality [36].

The driving force of diffusive transport of ions is the gradient of the electrochemical potential

$$\mu^{\alpha}(\mathbf{r}) = \mu_c^{\alpha}(\mathbf{r}) + q^{\alpha}\Phi(\mathbf{r}), \tag{1}$$

where $\mu_c^{\alpha}(\mathbf{r})$ is the chemical potential of species α, q^{α} is the charge of the ion, and $\Phi(\mathbf{r})$ is the mean electrostatic potential. The first term can be identified with the chemical work necessary to bring the ion from infinity to position $\mathbf{r}$, while the second term can be identified with the electrical work. These two terms, of course, cannot be separated experimentally. In calculations, however, they can be distinguished to better understand the behavior of the system.

Steady-state transport is maintained if the difference in the chemical potentials (concentration difference) and/or electrical potentials (voltage) is maintained on the two sides of the membrane. This means prescribed boundary conditions (BCs) in μ_c^{α} and Φ on the boundaries of the system. A well-established method to maintain these differences in the intensive variables is the Dual Control Volume (DCV) method, where two control cells are defined on the two sides of the membrane [37,38]. Given concentrations are established in the control cells by GCMC simulations. Between the two control cells (e.g., in the transport region), the system is simulated with one of the dynamical simulation methods (MD, LD, BD, or DMC); the mechanistic description of the system is reserved in this region. That is, only the control cells are connected to baths with well-defined thermodynamic variables via MC simulations performed in a given statistical mechanical ensemble. This is made possible by the assumption that the control cells are in thermodynamic equilibrium.

The disadvantage of this setup, however, is that it is inefficient in certain situations, for example, when a given species is present in very small concentrations. This is an important case for Ca channels in both experiments (Ca^{2+} is added gradually, starting with very low concentrations) and in the physiological situations (Ca^{2+} is present in the extracellular space in mM concentration). Simulation of this case with the DCV method is problematic, because the event that a Ca^{2+} enters the channel from the dilute bath is a rare event, which makes the sampling inadequate.

The idea to overcome this difficulty is not to wait for a particle to enter the transport region from the dilute bath, but rather insert (or delete) the particle into this region with a certain probability [39]. In practice, we divide the space into small volume elements and adopt the formalism of GCMC simulations, inserting/deleting particles with the acceptance probabilities of the GCMC technique. This probability is different for the various volume elements containing a $\mu^{\alpha}(\mathbf{r}_i)$ parameter for species α and volume element i. This parameter can be identified with the local chemical potential in the given volume element as soon as we assume local equilibrium (LE) [40]. In the case of charged particles we must work with the electrochemical potential profile. Then, we perform independent GCMC simulations for the different volume elements. This method, called Local Equilibrium Monte Carlo (LEMC) provides the concentration profiles, $c^{\alpha}(\mathbf{r}_i)$, of the various species as the output of the simulation.

The control cells can be considered as large volume elements, where there are real thermodynamic equilibria and the identification of the $\mu^{\alpha}(\mathbf{r}_i)$ parameter with the (electro)chemical potential is exact.

The LEMC simulation establishes a relationship between $\mu^{\alpha}(\mathbf{r})$ and $c^{\alpha}(\mathbf{r})$, but it does not say anything about the dynamics of the system, namely, the flux carried by the various species, $\mathbf{j}^{\alpha}(\mathbf{r})$. Also, we do not have any assurance that the $\mu^{\alpha}(\mathbf{r})$ profile used as the input of the LEMC simulation is the correct chemical potential profile. Therefore, we need an additional theory that (1) describes the dynamics of the system and (2) provides a closure between $\mu^{\alpha}(\mathbf{r})$ and $c^{\alpha}(\mathbf{r})$.

This additional theory can be simply a transport equation. We have proposed coupling the LEMC technique with the Nernst–Planck (NP) equation [39], where the flux is computed from

$$-kT\mathbf{j}^{\alpha}(\mathbf{r}) = D^{\alpha}(\mathbf{r})c^{\alpha}(\mathbf{r})\nabla\mu^{\alpha}(\mathbf{r}), \tag{2}$$

where $D^{\alpha}(\mathbf{r})$ is the diffusion coefficient profile, k is the Boltzmann-constant, and T is the temperature (298.15 K, in this work). In the resulting NP + LEMC method [39], the chemical potential is iterated until conservation of mass ($\nabla \cdot \mathbf{j}^{\alpha}(\mathbf{r}) = 0$) is satisfied (this provides the required closure).

The closure can also be provided by a direct dynamical simulation method (MD, LD, BD, or DMC). As a first step, we have coupled the LEMC method to the DMC technique [41]. In this case, the flux is provided by the DMC simulation, and the job of the LEMC technique is to maintain the constant driving force for the steady-state transport. An iteration procedure is still necessary to satisfy the continuity equation. It is a generalization of the control cell method; LE is assumed everywhere, not only in the control cells.

In this paper, we apply the NP + LEMC method to a reduced model of the Ca channel. In this reduced model, only the terminal groups of the side chains of the relevant amino acids of the selectivity filter are modeled explicitly. These amino acids have been identified as the determining factors in the channels' selectivity properties with point mutation experiments [10]. This type of reduced models was successfully used previously to qualitatively reproduce the micromolar Ca^{2+}-block in the L-type Ca channel [25,42–44]. A similar, but more detailed model was used by Gillespie for the RyR Ca channel [28–30], who studied this model with the NP equation coupled to a Density Functional Theory (NP + DFT). He successfully reproduced hundreds of current–

voltage curves and predicted anomalous Ca^{2+} concentration dependence (called Anomalous Mole Fraction Effect, AMFE) before it was actually measured.

AMFE is a fingerprint of strong divalent vs. monovalent selectivity [30,42]. In this work, we apply the simple channel model used for the L-type Ca channel to qualitatively reproduce AMFE curves for the RyR Ca channel. Because this model is more simplistic than that of Gillespie, we expect only qualitative agreement. We want to demonstrate the capabilities of the NP + LEMC technique to work in asymmetric ionic conditions with low concentrations in the presence of external voltage. The experimentally motivated cases for the RyR channel make it possible to connect to reality to some degree instead of just running simulations for a general channel model. The other advantage of using the RyR channel as a test case is that the NP + DFT calculations of Gillespie proved that the mechanism behind the reduced model (competition of electrostatic attraction and hard sphere repulsion) is sufficient to reproduce experimental data for this type of channel.

The diffusion coefficient profile, which is an input of the NP + LEMC calculation, is estimated on the basis of DMC + DCV simulation data by fitting the $D^{\alpha}(\mathbf{r})$ values so that we reproduce the flux ratio data (dynamical selectivity) obtained from the DMC + DCV simulation. With this, we demonstrate how we can couple two different simulation techniques by getting dynamical information from the DMC simulation and using it in the transport equation.

2. Model

The geometry of our system is shown in Fig. 1. The simulation cell has rotational symmetry, so, our cell has a cylindrical shape obtained by rotating the shape of Fig. 1 around the z-axis. The cell is confined by hard walls; no periodic BCs are applied. A membrane defined by two planar hard walls is placed in the middle of the cell; the thickness of the membrane is 20 Å. A pore penetrates this membrane representing the pore of the channel protein. The pore has rounded edges at the entrances of 5 Å curvature radius forming vestibules to the central cylindrical region (of length 10 Å) of the pore. This central region represents the selectivity filter of the channel. The radius of the selectivity filter, denoted by R, is an important parameter from the point of view of selectivity [21,26]. The two regions outside the membrane on both sides represent the two baths. Distinction of access and bulk regions is necessary for the NP + LEMC technique as explained in the next section.

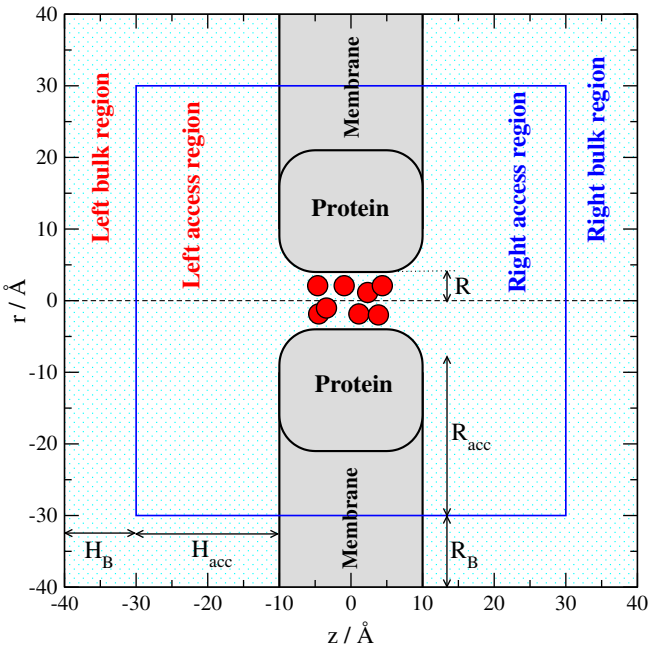

Fig. 1. Geometry of the simulation cell. It is a cylinder confined by hard walls. The cell is obtained by rotating the shape in the figure around the z-axis. A membrane with a channel is placed in the center between -10 Å $< z <$ 10 Å. The central cylindrical part (-5 Å $< z <$ 5 Å) of the channel represents the selectivity filter of radius R. The solution domain of the NP + LEMC system includes the channel region and the access regions. The outer boundary surface of this domain (indicated by the blue line) is denoted by $\mathcal{B}$. The dimensions of the access regions are characterized by H_{acc} and R_{acc}. There are bulk regions outside the solution domain, but still inside the simulation cell with dimensions H_B and R_B.

The selectivity filter contains eight half charged oxygen ions, $O^{1/2-}$, representing the oxygen atoms of the COO^- groups hanging at the end of the side chains of the four aspartic amino acids identified in the selectivity filter of the RyR Ca channel. In the case of the L-type Ca channel, these are four glutamic acids (EEEE locus). These amino acids have been identified with point mutation experiments; changing them, for example, to small and neutral alanine (A), the selectivity properties of the channel are drastically altered [10]. This model was used in our earlier GCMC [20,21,23,26,27,45] and DMC [19] studies to describe Ca channels in general, and later, to model the L-type Ca channel specifically [25,42,43]. In the case of the RyR Ca channel, even more amino acids have been identified in and near the selectivity filter that made it possible for Gillespie to construct his detailed channel model [28–30] used in his NP + DFT calculations. In this paper, however, we focus on qualitative agreement and testing our newly introduced NP + LEMC method, so we use the simpler model shown in Fig. 1.

The oxygen ions are modeled by charged hard spheres of diameter 2.8 Å. Because the side chains of the amino acids in the filter are hanging inside the pore in the permeation pathway [10] and they are relatively long and flexible, we assume that the terminal groups are mobile. This assumption was first made by Nonner et al. [12] in their Mean Spherical Approximation calculations and it is the basis of the Charge-Space Competition (CSC) mechanism [46]. This mechanism states that in the small and crowded (with amino acid side chains) selectivity filter, ionic selectivity in a Ca channel is driven by a competition between ions based on their two essential features: their charge and size. These two features allow the filter to distinguish between the ions using two essential physical forces: electrostatic attraction and volume exclusion. Specifically, the selectivity filter of the Ca channel prefers the divalent Ca^{2+} ions over the monovalent Na^+ ions because they provide twice the charge in the same volume to balance the negative charge of the oxygen ions in the filter. The mechanism can also interpret selectivity between ions of the same valence but different diameter [25,27,47,48] and selectivity in sodium channels [22,44,49]. The strongest support of the mechanism is presumably the success of Gillespie in reproducing hundreds of current–voltage data for the RyR channel in varying conditions.

The ions are modeled as charged hard spheres, with diameters 1.9, 1.98, and 3.62 Å for Na^+, Ca^{2+}, and Cl^-, respectively. Water is modeled as a dielectric continuum with dielectric constant $\epsilon = 78.5$ throughout the system (meaning, in the bath, in the pore, and inside the membrane). This is the Primitive Model of electrolytes, which was shown to be quite "non-primitive" because it can reproduce the non-monotonic concentration dependence of the activity coefficients of electrolytes [50]. The concentration dependence of the dielectric constant plays a central role in this theory.

The strong Ca^{2+} vs. Na^+ selectivity of the L-type Ca channel could be reproduced by assigning a different dielectric constant (usually $\epsilon_{pr} = 10$) to the interior of the protein/membrane region (gray area in Fig. 1) [20,21,25,27,42,43]. The dielectric boundaries forming such systems carry induced charges whose calculation was solved with our Induced Charge Computation (ICC) method [20,51].

The RyR Ca channel, however, is a weakly-selective channel and using uniform dielectric constant proved to be sufficient in the model of Gillespie. Therefore, we do not include dielectric inhomogeneities

in this study. Another aspect that gives a different flavor to Gillespie's model is that he used neutral hard spheres to represent the corpuscular nature of water molecules. This is the Solvent Primitive Model that was used by several investigators in various situations [52–58].

During the years, many aspects of this channel model have been investigated with GCMC simulations. We have studied the effect of protein dielectric constant [20,27], channel radius [21], channel shape [26], fixing or restricting the mobility of oxygen ions [45], putting the oxygen ions behind the wall buried in the body of the protein [23], and the presence of trivalent ions [43]. Most importantly, free energy studies have been published where the effects of various components of the excess chemical potential (hard sphere, electrostatic, mean field, ionic, polarization, etc.) have been separated for the RyR Ca channel [29] and the L-type Ca channel [27]. All these studies showed that the model can produce very diverse selectivity properties by adjusting only a handful of model-parameters, explaining the basic selectivity mechanisms of various ion channels (L-type and RyR Ca channels, DEKA Na channel).

3. Methods

First, we describe the LEMC method, then we show how we couple it to the NP transport equation. Lastly, we briefly outline the DMC + DCV method, which we used to get information about the diffusion coefficient values in the selectivity filter.

3.1. The Local Equilibrium Monte Carlo method

The LEMC method considers a finite system with prescribed BCs on the boundaries. Specifically, the system depicted in Fig. 1 considers different chemical and electrical potentials in the bulk regions on the left and right hand sides: $\mu^{\alpha}_{c,L}$ and Φ_L on the left, while $\mu^{\alpha}_{c,R}$ and Φ_R on the right. The difference of the electrical potentials defines the applied voltage:

$$\Delta\Phi = \Phi_L - \Phi_R. \tag{3}$$

The bulk chemical potentials of the various species, $\mu^{\alpha}_{c,L}$ and $\mu^{\alpha}_{c,R}$, for a given composition (prescribed concentrations c^{α}_L and c^{α}_R for every species α) of the electrolyte are calculated with the Adaptive GCMC method of Malasics et al. [59,60]. It is important to stress that the concepts of chemical and electrical potentials are used only in the bulk regions at the boundaries of the system because in experiments we set electrolyte composition and voltage. In the LEMC technique and in the NP equation, however, we use the electrochemical potential as a variable, so we set the BCs for this variable:

$$\begin{aligned}\mu^{\alpha}_L &= \mu^{\alpha}_{c,L} + q^{\alpha}\Phi_L \\ \mu^{\alpha}_R &= \mu^{\alpha}_{c,R} + q^{\alpha}\Phi_R.\end{aligned} \tag{4}$$

The boundary of the transport region is indicated by blue line in Fig. 1 (denoted by $\mathcal{B}$). The regions between the bulk regions and the channel are called access regions. In the access regions, double layers are formed that strongly influence the behavior of the system contributing to the total resistance.

In the transport region (inside $\mathcal{B}$), the electrochemical potential is not constant and the system is out of equilibrium. The basic assumption of the LEMC method is that we can simulate this region with the toolbox of the equilibrium MC simulation technique. Specifically, we divide the transport region into small volume elements, $\mathcal{D}_i$, that are considered separately as individual simulation cells. Separate GCMC simulations are performed for these elementary cells. The acceptance probability of particle insertion/deletions into/from such a cell is $min(1, p^{\alpha}_{i,\chi}(\mathbf{r}))$, where

$$p^{\alpha}_{i,\chi}(\mathbf{r}) = \frac{N^{\alpha}_i! V_i^{\chi}}{(N^{\alpha}_i + \chi)!} \exp\left(-\frac{\Delta U(\mathbf{r}) - \chi\mu^{\alpha}_i}{kT}\right). \tag{5}$$

In this equation, N^{α}_i is the number of ions of type α in the ith elementary cell before insertion/deletion, $\Delta U(\mathbf{r})$ is the energy change associated with the insertion/deletion in position $\mathbf{r}$, V_i is the volume of $\mathcal{D}_i$, while $\chi = 1$ for insertion, and $\chi = -1$ for deletion. The variable μ^{α}_i can be identified with the local electrochemical potential as soon as LE is assumed. If the assumption of LE is problematic [40], the $\mu^{\alpha}(\mathbf{r})$ variable is just an adjustable quantity that controls the local concentration in the transport region. The assumption of LE, therefore, is not necessary to apply the LEMC technique. We identify $\mu^{\alpha}(\mathbf{r})$ with the function whose gradient drives the transport when we couple the LEMC method to the NP transport equation. This identification is reasonable because using an empirical equation already assumes using various approximations: assuming LE and identifying $\mu^{\alpha}(\mathbf{r})$ with the local electrochemical potential is the least of our problems (the diffusion coefficient profile, for example, is quite an obscure quantity).

When we displace an ion from position $\mathbf{r}$ to position $\mathbf{r}'$, the Boltzmann factor in the acceptance probability can be given as

$$p^{\alpha}_{i\to j}(\mathbf{r},\mathbf{r}') = \exp\left(-\frac{\Delta U(\mathbf{r},\mathbf{r}') - \left(\mu^{\alpha}_j - \mu^{\alpha}_i\right)}{kT}\right), \tag{6}$$

where the difference $\mu^{\alpha}_j - \mu^{\alpha}_i$ expresses the work that we have to exert to move the ion against the electrochemical potential difference. This term appears if position $\mathbf{r}$ is in cell i and position $\mathbf{r}'$ in cell j.

The energy change ΔU in the above equation contains the direct interactions with all the ions in the whole simulation cell. The system outside the elementary simulation cell, $\mathcal{D}_i$, therefore, exerts its effect on the ion(s) in $\mathcal{D}_i$ as an external constraint. This constraint, of course, changes as the simulation evolves because the ions outside $\mathcal{D}_i$ also move. The energy change ΔU also contains the interaction with an external electrical potential, $\Phi^{appl}(\mathbf{r})$. This applied potential is the result of the Dirichlet BCs prescribed on the system's boundaries (Φ_L and Φ_R) and can be calculated solving Laplace's equation

$$\nabla^2\Phi^{appl}(\mathbf{r}) = 0 \tag{7}$$

for the transport region with the prescribed BCs. We solve this equation with the ICC method [20,51]. This method provides the induced charges on the system's boundary, $\mathcal{B}$, that produce the required potential profile inside $\mathcal{B}$. Interaction with the applied potential then can be computed from the interactions with these induced charges using Coulomb's law. Details are found in Appendix A.

In the present geometry, the elementary cells are $\Delta z \times \Delta r$ rectangles in the (z,r) plane. In the three-dimensional space, these correspond to concentric rings with the z-axis in their centers.

The output of the LEMC simulation is the average number of the ions of species α in the elementary cell $\mathcal{D}_i$ denoted by $\langle N^{\alpha}_i\rangle$. The density (concentration, if we prefer that unit) of ions then can be obtained by dividing with the volume of the elementary cell: $c^{\alpha}_i = \langle N^{\alpha}_i\rangle / V_i$. However, it proved to be more advantageous to use the Widom particle insertion method [61,62] also known as the Potential Distribution Theorem [63,64]. According to this theorem, the excess chemical potential can be computed as

$$e^{-\mu^{\alpha,EX}_i/kT} = \left\langle e^{-\Delta U^{\alpha}_i/kT}\right\rangle, \tag{8}$$

where ΔU^{α}_i is the energy change associated with the insertion of a particle of species α into a randomly chosen position in the elementary cell i. This is the same energy computed in the particle insertion step of the

LEMC technique, therefore, it does not require additional computational cost. Since the excess chemical potential is defined as

$$\mu_i^{\alpha,\mathrm{EX}} = \mu_i^{\alpha} - kT \ln c_i^{\alpha}, \tag{9}$$

the concentration can be expressed as

$$c_i^{\alpha} = \left\langle e^{-\Delta U_i^{\alpha}/kT} \right\rangle e^{\mu_i^{\alpha}/kT} \tag{10}$$

from Eqs. (8) and (9). In these equations (and in every equation in this paper), μ_i^{α} denotes the configurational part of the electrochemical potential, which does not include the term with the de Broglie thermal wavelength.

We have checked that this method works in the non-equilibrium situation considered in the LEMC framework. The ΔU_i^{α} energy contains the interaction with the applied field and μ_i^{α} is the local electrochemical potential assigned to the elementary cell $\mathcal{D}_i$. The concentration is the same obtained from Eq. (10) as that obtained from counting the ions in the usual way, but much more accurate. The explanation is that in some elementary cells the concentration is so small that it is a rare event that an ion is found there. Sampling using the conventional method, therefore, is less efficient. Sampling using Eq. (10), on the other hand, is more efficient, because the energy ΔU_i^{α} always has a value, which contributes to sampling at every insertion.

3.2. Iteration using the Nernst–Planck equation and conservation of mass

The LEMC technique provides discrete c_i^{α} output values for the discrete μ_i^{α} input values. These concentration values are assigned to the centers of the volume elements, $\mathbf{r}_i$. Their values can be computed anywhere in the simulation cell by linear interpolation. Similarly, the electrochemical potential and its gradient can be computed anywhere in the simulation cell numerically. Provided that we have the value of the diffusion coefficient everywhere in the cell, we can compute the flux density, $\mathbf{j}^{\alpha}(\mathbf{r})$, from the NP equation (Eq. (2)). The resulting flux density should satisfy the continuity equation

$$\nabla \cdot \mathbf{j}^{\alpha}(\mathbf{r}) = 0, \tag{11}$$

namely, conservation of mass. Because there is no any guarantee that the input electrochemical potentials produce concentrations (through the LEMC simulations) that, together, produce flux densities (through the NP equation) that satisfy the continuity equation, we use an iteration technique that iterates the electrochemical potential until the conservation of mass is satisfied.

Technically, we use the divergence theorem to obtain a surface integral over the closed surface of volume element $\mathcal{D}_i$:

$$0 = \int_{\mathcal{D}_i} \nabla \cdot \mathbf{j}^{\alpha}(\mathbf{r}) dV = \oint_{\mathcal{S}_i} \mathbf{j}^{\alpha}(\mathbf{r}) \cdot \mathbf{n}(\mathbf{r}) da, \tag{12}$$

where $\mathcal{S}_i$ denotes the surface and $\mathbf{n}(\mathbf{r})$ is the normal vector pointing outward at position $\mathbf{r}$ of the surface. The $\mathcal{S}_i$ surface is then divided into surface elements $\mathcal{S}_{ij}$ that form the interfacial surface element between volume elements $\mathcal{D}_i$ and $\mathcal{D}_j$. We assume that the concentration, the gradient of the chemical potential, the diffusion coefficient, and the flux density is constant at these surface elements. They will be denoted by hat: $\hat{c}_{ij}^{\alpha}$, $\nabla\hat{\mu}_{ij}^{\alpha}$, $\hat{D}_{ij}^{\alpha}$, and $\hat{\mathbf{j}}_{ij}^{\alpha}$. The integral in Eq. (12), then, is written as a sum over the surface elements

$$0 = \sum_{j,\ \mathcal{S}_{ij} \in \mathcal{S}_i} \hat{\mathbf{j}}_{ij}^{\alpha} \cdot \mathbf{n}_{ij}\ a_{ij}, \tag{13}$$

where a_{ij} is the area of surface element $\mathcal{S}_{ij}$.

The iteration algorithm can be given as follows.

1. We begin with an appropriately chosen initial set of electrochemical potentials, $\mu_i^{\alpha}[1]$, and compute the linearly interpolated values at the $\mathcal{S}_{ij}$ surface elements. The numbers in square brackets denote the sequential number of the iteration.
2. LEMC simulations are performed using these values as inputs. The resulting concentrations are denoted by $c_i^{\alpha}[1]$.
3. Electrochemical potential values for the next iteration are obtained on the basis of the assumption that the flux computed from the "old" concentrations $c_i^{\alpha}[1]$ and the "new" electrochemical potentials $\mu_i^{\alpha}[2]$ satisfy Eq. (13). For a general $[n] \to [n+1]$ iteration, we obtain

$$0 = \sum_{j,\ \mathcal{S}_{ij} \in \mathcal{S}_i} \hat{D}_{ij}^{\alpha}\ \hat{c}_{ij}^{\alpha}[n] \nabla\hat{\mu}_{ij}^{\alpha,\mathrm{CAL}}[n+1] \cdot \mathbf{n}_{ij}\ a_{ij}. \tag{14}$$

   The values $\nabla\hat{\mu}_{ij}^{\alpha,\mathrm{CAL}}[n+1]$ are obtained from the $\mu_i^{\alpha,\mathrm{CAL}}[n+1]$ values by linear interpolation (the superscript CAL indicates that we calculate the electrochemical potential values from Eq. (14)). Therefore, Eq. (14) is a system of linear equations with the $\mu_i^{\alpha,\mathrm{CAL}}[n+1]$ values being the unknowns. We have such an equation for every volume element with an unknown electrochemical potential for each, so the system of linear equations is solvable. BCs enter Eq. (14) when we write it up for elementary cells bordering $\mathcal{B}$. More details about the solution are found in the supplementary material of Ref. [39].
4. We found that in the case of large driving forces we obtain faster and more robust convergence using a mix of the values calculated in the $[n+1]$th iteration and the values obtained in the $[n]$th iteration by mixing:

$$\mu_i^{\alpha,\mathrm{MIX}}[n+1] = \beta^{\alpha}\mu_i^{\alpha,\mathrm{CAL}}[n+1] + (1-\beta^{\alpha})\mu_i^{\alpha,\mathrm{MIX}}[n]. \tag{15}$$

   The parameter β^{α} determines in what ratio we use the two values in the mixing. If this parameter is close to 0, the iteration is more steady, but it is slow because the electrochemical potential values change slowly during the iteration. Increasing the value of β^{α}, we can get faster iteration, but we must be aware of the danger that the system can be trapped in fluctuating between local minima. In our calculations, we found the values $\beta^{\alpha} = 0.9 - 0.95$ for ± 20 mV, and $\beta^{\alpha} = 0.7 - 0.8$ for ± 100 mV appropriate.
5. The values $\mu_i^{\alpha,\mathrm{MIX}}[n+1]$ are used as the input of the LEMC simulations of the next round.

Practically the same iteration technique was used by Gillespie in his NP + DFT calculations with the difference that there the concentration was iterated and the chemical potential was computed from DFT (the reverse of the GCMC route). Because DFT provides well-defined numbers for a given set of input concentrations, the iteration procedure converges and provides a well-established solution.

In the case of simulations, however, the solution is always obtained within a statistical error. The iteration, therefore, does not converge to a given solution, but fluctuates around it. Therefore, we obtain the final solution by averaging over the iterations. We found it more suitable to run shorter LEMC simulations in more iterations. The running average obtained this way can reach arbitrary accuracy.

At the end of this procedure, the flux densities of the diffusing ionic species are obtained. According to the rotational symmetry, vector $\mathbf{j}^{\alpha}(\mathbf{r})$ is described with two components in the (z,r) plane: $j_z^{\alpha}(z,r)$ and $j_r^{\alpha}(z,r)$. The net flux through a cross section of radius $R(z)$ of the pore is calculated as

$$J^{\alpha}(z) = 2\pi \int_0^{R(z)} r\, j_z^{\alpha}(z,r)\, dr. \tag{16}$$

This value is constant (denoted by J^{α}) inside the pore ($|z| < 10$ Å) because the ions are not allowed to leave the pore in the radial direction.

The electrical current carried by an ionic species is then $I^\alpha = q^\alpha J^\alpha$ and the total current is

$$I = \sum_\alpha q^\alpha J^\alpha. \tag{17}$$

3.3. Dynamic Monte Carlo with dual control volumes

The diffusion constant profile is an input for the NP + LEMC calculation. This quantity includes all the dynamical information about the mobility of ions in the various regions. To complete the NP + LEMC calculation, therefore, we need some information about the diffusion coefficients. In the baths, the diffusion constants of the various ionic species are usually experimental data. In the channel, however, this information is not readily available. There are two ways to get this information. First, we can fit them to experimental data as Gillespie did in his NP + DFT calculations [28–30]. This route is appropriate if we study an experimental situation. In the case of model calculations, where direct connection to experiments is not present, we can get the dynamical information from direct dynamical simulations.

In this work, we follow a mixture of the two approaches. We use the value of the diffusion coefficient of Na^+ in the filter, $D_F^{Na^+}$, as obtained by Gillespie for the RyR channel. The value of $D_F^{Na^+}$ in itself does not influence selectivity; it rather just modulates the absolute value of current flowing through the channel. The diffusion coefficient of Ca^{2+} in the filter (more precisely, the $D_F^{Ca^{2+}}/D_F^{Na^+}$ ratio), on the other hand, directly determines selectivity, which is our main concern in this work. Fitting to experimental data has already been tested in Gillespie's works [28–30]. Here we are rather interested in the question whether using the $D_F^{Ca^{2+}}/D_F^{Na^+}$ value obtained from calculations for the model gives sensible results for the experimental situation. We generally make efforts to minimize the number of adjustable parameters of a model. If a piece of information can be gained from the model itself, it can be considered as an "internal" parameter. Therefore, it is sensible to use this "internal" parameter instead of obtaining it from an "external" source. Our results imply that the $D_F^{Ca^{2+}}/D_F^{Na^+}$ ratio can be considered as such an "internal" parameter, because the mobilities of ions in the selectivity filter are largely determined by local interactions between particles modeled explicitly.

Our choice of the direct dynamical simulation method to obtain $D_F^{Ca^{2+}}$ is the DMC technique, because it proved to be computationally more efficient than the LD method, which is DMC's natural alternative for this implicit water system. DMC provides better sampling and also handling of hard sphere and hard wall interactions is much easier in it.

The basic DMC step is the random particle displacement, in which one particle is chosen from the N particles available in the system with $1/N$ probability, and it is moved into a new position within a maximum displacement (the usual MC particle displacement). The DMC method is based on the assumption that the sequence of configurations generated by the above steps can be considered as a dynamic evolution of the system in time [65]. DMC, however, does not generate deterministic trajectories; it reproduces average dynamic properties such as the mean square displacement. Compared to MD, DMC does not guarantee an absolute measure of physical time; it only ensures proportionality, which makes it an appropriate candidate to simulate selectivity. In the DMC technique [66], the flux, J^α, is calculated by counting the net movement of particles from-left-to-right and from-right-to-left through selected reference planes perpendicular to the z-axis for a given length of the simulation. The computed number is divided by the square root of the mass of the component [36] since DMC in itself does not reflect mass dependence.

The key parameter of the algorithm is the maximum displacement r_{max}. For systems with every component modeled explicitly, the value of r_{max} can be determined from the average free path of molecules as shown by Rutkai and Kristóf [36]. The property that determines the value of r_{max} in the first order is the density of the fluid. The algorithm of Rutkai and Kristóf [36] was justified by comparing to results of MD simulations. The case of implicit solvent, on the other hand, is not so obvious because the value of r_{max} must reflect not only the collision with other solute particles but also with water. Therefore, r_{max} should be kept at a small value (≈ 1 Å) to mimic (at least partially) the stochastic random walk of particles among the solvent molecules.

The DMC simulation is performed for the transport region between two control cells (basically corresponding to the bulk regions in Fig. 1). In this DCV method, the driving force is maintained by the concentration difference between the control cells.

DMC simulations do not give information about the number of particles passing the reference plane in one second. Simulation time can be connected to real time by fitting to experiments. The ratio of fluxes carried by the two components (J^α/J^β, dynamical selectivity), however, is a well-defined quantity (it is dimensionless) and it is the major output of the simulation. This quantity is the essential link between the various methods (MD + DCV, DMC + DCV, DMC + LEMC) that are said to be consistent if they give the same result for the dynamical selectivity [41]. In this work, the diffusion coefficient of Ca^{2+} in the filter is chosen so that the NP + LEMC method reproduces the J^α/J^β value given by the DMC + DCV method.

4. Results

We present results for two different situations:

1. In previous work by Rutkai et al. [19], we studied a general Ca channel model using DMC + DCV simulations. In those simulations, we performed a mole fraction experiment, where a mixture of NaCl and $CaCl_2$ was present at different compositions, but at fixed total concentration of the cations, $C_L^{Na^+} + C_R^{Ca^{2+}} = 10$ mM. We studied the correlation between binding affinity and dynamical selectivity in that work. Here, we use this case to investigate the role of various geometrical parameters, such as the size of bulk regions (H_B and R_B), the size of the access regions (H_{acc} and R_{acc}), and the grid resolution used to solve the NP + LEMC system. The mole fraction experiment of Rutkai et al. [19] is repeated and analyzed to see how the results change with these parameters.
2. The other system is supposed to mimic the RyR Ca channel. In this case, we perform computer experiments inspired by real electrophysiological experiments on the RyR channel: $CaCl_2$ is added to a constant background of NaCl at different voltages. We will study the effect of NaCl concentrations and voltages.

In both cases, the diffusion coefficient profiles, $D^\alpha(z)$, were constructed as follows. They are assumed to be independent of r. We used fixed values outside the membrane region ($|z| > 10$ Å), denoted by D_B^α, and in the selectivity filter ($|z| < 5$ Å) denoted by D_F^α. In the vestibules (5 Å < $|z|$ < 10 Å), we used a linear interpolation between D_F^α and D_B^α.

The values outside the membrane region are the experimental bulk values. For the cations, they are $D_B^{Na^+} = 1.33 \times 10^{-9}\ m^2 s^{-1}$ and $D_B^{Ca^{2+}} = 7.92 \times 10^{-10}\ m^2 s^{-1}$.

Thus, the only adjustable values are those in the selectivity filter. Because the DMC + DCV simulation gives information only about the flux ratio, we cannot adjust both $D_F^{Na^+}$ and $D_F^{Ca^{2+}}$. Therefore, we used the value $D_F^{Na^+} = 3.92 \times 10^{-11}\ m^2 s^{-1}$ as reported by Gillespie [30]. The order of magnitude of the diffusion coefficients in the filter tunes the order of magnitude of the currents carried by the various ions; they have less effect on selectivity, which is our main interest.

Therefore, we do not care about the order of magnitude of the values in the filter too much. Selectivity is rather influenced by the ratio of the diffusion coefficients of the two competing species in the filter: $D_F^{Ca^{2+}}/D_F^{Na^+}$. This ratio will be fitted to the $J^{Ca^{2+}}/J^{Na^+}$ result given by the DMC + DCV simulation.

4.1. Effect of geometrical parameters

We start with the selectivity filter of the channel model considered in the work of Rutkai et al. [19] with a radius $R = 4$ Å. The total cation concentration on the left hand side is 100 mM, while it is 33 mM on the right hand side (with the same mole fraction as on the left). The driving force of the transport is the concentration difference, namely, the chemical potential gradient.

We have chosen the Ca^{2+} mole fraction value 0.2 (this corresponds to $c_L^{Ca^{2+}} = 20$ mM) to fit the diffusion coefficient. At this mole fraction, the flux ratio given by DMC + DCV is $J^{Ca^{2+}}/J^{Na^+} \approx 1.64$. We found that this value is reproduced when $D_F^{Ca^{2+}}/D_F^{Na^+} \approx 0.5$.

These two numbers already characterize the relation between binding and dynamical selectivity: although the mobility of Ca^{2+} is smaller in the channel, its flux is larger. Moreover, the driving force is smaller for Ca^{2+} (the chemical potential difference between the two sides of the membrane for Na^+ and Ca^{2+} are 0.89 kT and 0.26 kT, respectively) and there are four times fewer Ca^{2+} in the bulk than Na^+. The result of the Ca^{2+}-flux being larger is then possible only if Ca^{2+} is present in the channel in much larger number than Na^+ is. That is, binding selectivity favors Ca^{2+} over Na^+.

4.1.1. The effect of the bulk region

The simulation cell does not necessarily coincide with the solution domain of the NP + LEMC system. The former contains bulk regions just outside the latter (see Fig. 1), where the chemical potentials and electrical potentials have constant values ($\mu^{\alpha}_{c,L}$, $\mu^{\alpha}_{c,R}$, Φ_L, and Φ_R). These regions practically correspond to the control cells used in the DCV technique. Therefore, we assume real thermodynamic equilibria there.

We have found that the size of this region must be large enough to accommodate the interfacial region of the electrolyte appearing near the outer confining hard wall of the system. At such a boundary, the electrolyte system shows depletion, namely, the concentration of ions near the wall is smaller than in the bulk far from the wall. In the absence of the bulk region ($H_B = R_B = 0$), therefore, this depletion layer appears in the access region. In this case, $\mathcal{B}$ is not only an imaginary surface indicating the boundary of NP + LEMC solution domain, but it is also a hard wall. This makes the concentration smaller at $\mathcal{B}$ than its real bulk value, making the flux smaller through $\mathcal{B}$ because the flux is proportional to the concentration (Eq. (2)). Because the total number of particles passing through $\mathcal{B}$ in unit time (the integral of the flux density over the surface) must be the same as in the pore, a smaller flux at $\mathcal{B}$ corresponds to a smaller flux through the channel. The calculations show that this is the case: we obtain smaller flux using bulk regions of insufficient size (data not shown).

4.1.2. The effect of the access region

The access region (its dimensions are denoted by H_{acc} and R_{acc}) is positioned between the bulk region and the channel region. This region is very important because it accommodates the interfacial layers formed on the two sides of the membrane. These layers are especially important when a voltage is applied; in this case, they are called double layers. Cations are present in smaller or larger number in the double layers compared to the bulk values depending on the sign of voltage. The structure of the double layer, therefore, strongly influences the resistance of the access region for a given ionic species. Appropriately-sized access regions, therefore, must be included in the model if we want a correct description of the system.

Here, we demonstrate the importance of the access region for zero voltage. When voltage is present, even larger access regions should be used (see Appendix A for more details). Fig. 2 shows the results for the studied case (0.2 Ca^{2+} mole fraction) using various values for $H_{acc} = R_{acc}$. The size of the bulk region is $H_B = R_B = 10$ Å. Quantities averaged over the cross section are plotted. In particular, the line density

$$n^{\alpha}(z) = 2\pi \int_0^{R(z)} c^{\alpha}(r,z)\, r\, dr \tag{18}$$

is the number of particles along the z-axis for a given unit length (top panel). The flux is constant in the channel because there is no net flux in the radial direction. Outside the channel, the $J_z^{\alpha}(z)$ profiles decline because the ions can leave the channel region in the radial direction along the membrane. This is a typical route for the ions; extra charge tends to stay near surfaces. The electrochemical potential (bottom panel) decreases monotonically. As seen, the size of the access region has a profound effect on all the functions appearing in the NP equation. The flux, therefore, is sensitive to the size of the access region, but it converges as we increase the size. This convergence is shown in Fig. 3 in terms of electrical currents carried by the two competing ions.

Fig. 2 also shows the line density profiles obtained from the DMC + DCV simulations. Inside the channel, it agrees well with the profiles given by the NP + LEMC technique. Furthermore, the NP + LEMC profiles coincide inside the channel independent of the size of the access

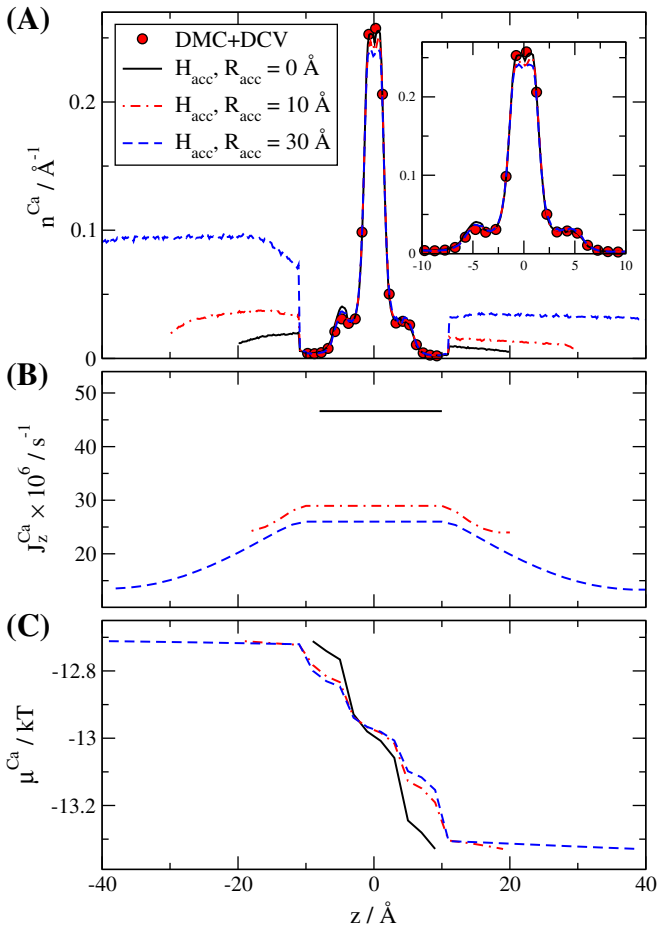

Fig. 2. Profiles for the (A) line number density, (B) z-component of the flux density, and (C) the electrochemical potential of Ca^{2+} for various dimensions of the access region (different lines correspond to NP + LEMC results obtained for different $H_{acc} = R_{acc}$ values). The bulk concentrations are $c_L^{Ca^{2+}} = 3c_R^{Ca^{2+}} = 20$ mM and $c_L^{Na^+} = 3c_R^{Na^+} = 80$ mM. No voltage is applied. The dimensions of the bulk regions are $H_B = R_B = 10$ Å. The symbols show the results of DMC + DCV simulations obtained with $H_{acc} = 0$ Å.

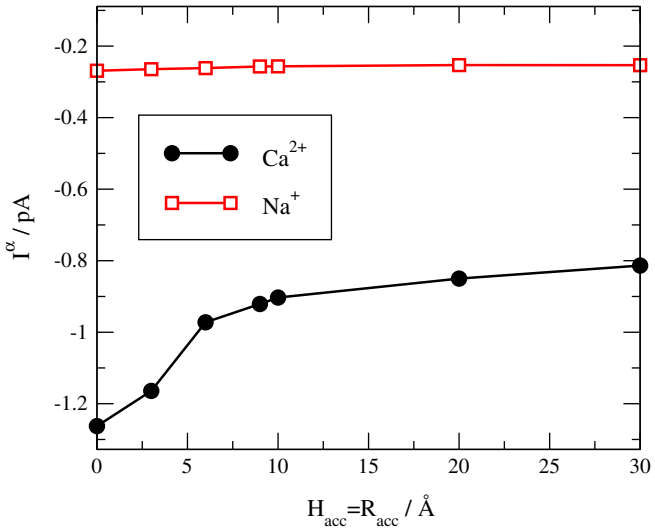

Fig. 3. The convergence of the currents, $I^{\alpha} = q^{\alpha}J^{\alpha}$, carried by Na^{+} and Ca^{2+} in terms of the size of the access regions. The system is the same as in Fig. 2.

region. This is because the ionic profiles in the channel are chiefly determined by local forces that are large compared to the effect of the ions in the access regions.

The access region of appropriate size is also necessary to satisfy the electrostatic (Dirichlet) BC imposed at $\mathcal{B}$ (see Appendix A for more details).

4.1.3. The effect of grid resolution

The NP + LEMC system is solved numerically for a grid of elementary cells formed by rectangles of size $\Delta z \times \Delta r$ in the (z,r) plane. A coarser grid means faster calculation, while a finer grid means more detail and more accuracy. In the latter case, the smaller volume elements require longer simulations for adequate sampling increasing computational time. We always have to compromise.

The question is how much accuracy do we lose with a coarser grid. Looking at the profiles computed with different resolutions in the range of $\Delta z = \Delta r = 0.8-2$ Å (results not shown) we can conclude the followings:

1. Large peaks in concentration profiles are lost using a coarser grid.
2. The electrochemical potential profiles are quite similar for various resolutions because they are smooth. The flux, however, depends on the gradient of the electrochemical potential. Small deviations, therefore, are magnified when we take the derivatives.
3. The flux of the respective ionic species, therefore, is quite sensitive to the resolution of the grid.
4. The ratio of the Ca^{2+} and Na^{+} fluxes, on the other hand, is insensitive to grid resolution because the change in grid resolution has a similar effect on both ions. Numerical results are shown in Table 1.

4.1.4. Mole fraction experiment

Lastly, we have performed the same mole fraction experiment that Rutkai et al. did using DMC + DCV simulations [19]. We used 10 Å for the dimensions of the bulk regions, $H_{acc} = 26$ Å and $R_{acc} = 20$ Å for the access region, and $\Delta z = \Delta r = 2$ Å for the resolution. We have performed calculations for Ca^{2+} mole fractions as small as 0.003. This demonstrates the advantage of the NP + LEMC method over the DMC + DCV method, which cannot give reasonable statistics for mole fractions smaller than 0.05. We could only extrapolate to that domain [19].

Table 1
Fluxes carried by the various ionic species for different resolutions of the grid (unit: 10^6 s^{-1}). The fourth column shows the dynamical selectiviy (flux ratio).

$\Delta z = \Delta r$	$J_z^{Ca^{2+}}$	$J_z^{Na^{+}}$	$J_z^{Ca^{2+}}/J_z^{Na^{+}}$
2.0	2.59	1.60	1.62
1.5	2.39	1.47	1.62
1.0	2.16	1.41	1.54
0.8	2.31	1.42	1.63

As Fig. 4 shows, NP + LEMC can handle small mole fractions easily. The top panel shows the electrical currents as carried by the two cations, as well as the total current. The AMFE (the minimum in total current vs. mole fraction curve) is clearly seen. It can be explained by the fact that the Na^{+}-current decreases faster than the Ca^{2+}-current increases. This is caused by several effects [30,42]:

1. Ca^{2+} replaces Na^{+} in the selectivity filter at very small mole fractions (see the bottom panel).
2. Ca^{2+}-current increases only moderately because it is present in other parts of the channel (the vestibules) in proportion with the mole fraction of Ca^{2+}.
3. An additional requirement is necessary to get the minimum: Na^{+}- and Ca^{2+}-currents at mole fractions 0 and 1 should be similar.

Note that although the diffusion coefficient was fitted to mole fraction 0.2, the agreement with the DMC + DCV results occurs for the whole mole fraction range.

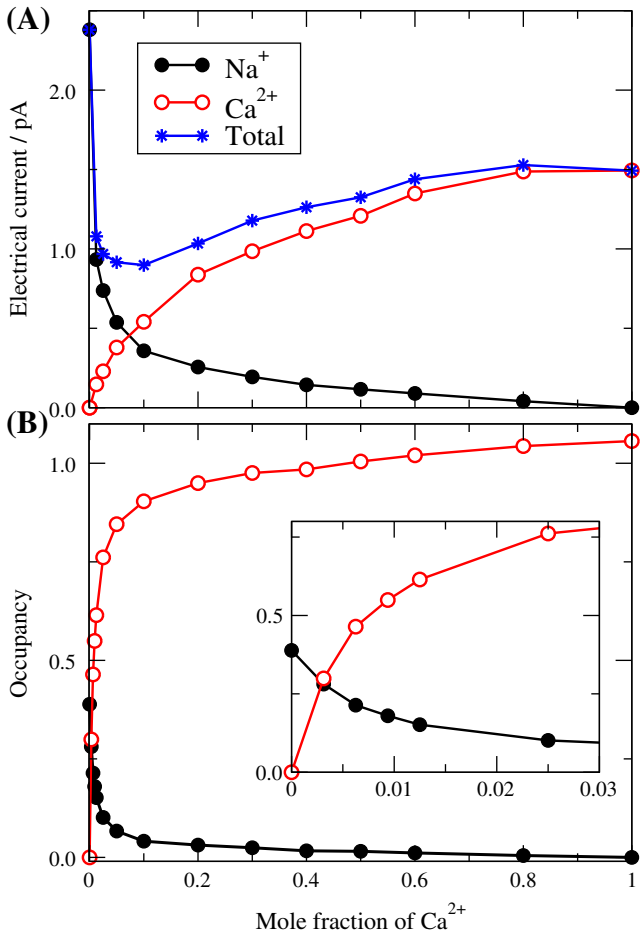

Fig. 4. NP + LEMC results for the mole fraction experiment simulated by Rutkai et al. [19] with DMC + DCV. The total concentration of Na^{+} and Ca^{2+} is 100 mM on the left hand side. The bulk concentrations are the third of these on the right hand side. Panel (A) shows the currents carried by the various cations and their sum, representing dynamical selectivity. Panel (B) shows the occupancies of the two cations (the average number of ions in the selectivity filter; e.g., the integral of the concentration profile) representing binding selectivity. The inset focuses on small mole fractions.

In summary, the channel binds Ca^{2+} more than it conducts it. In other words, Ca^{2+} vs. Na^+ binding selectivity is stronger than dynamical selectivity, a general conclusion for Ca channels [12,25,30,42].

4.2. Mole fraction experiments motivated by the RyR Ca channel

In the case of the model which is aimed to reproduce the experimental data for the RyR Ca channel qualitatively, the BCs for the NP + LEMC system are taken from the experiments. That is, we have NaCl on both sides of the membrane at concentrations $c_L^{Na^+} = c_R^{Na^+}$. $CaCl_2$ is added to the luminal side (this is, the sarcoplasmic reticulum side) of the membrane gradually ($c_L^{Ca^{2+}}$), while Ca^{2+} concentration on the cellular side is micromolar ($c_R^{Ca^{2+}} = 10^{-6}$ M). Voltage is set in a way that the ground is on the right hand (cellular) side.

For the radius of the selectivity filter we use the value $R = 4.5$ Å. This value was chosen by performing calculations for $R = 3.5$, 4, and 4.5 Å, and the mole-fraction curve for 4.5 Å was the one most similar to the experimental curve.

The diffusion coefficient of Ca^{2+} in the filter was again fitted to the results of DMC + DCV simulations for the same situation as in the previous subsection (100 mM total cation concentration, $c_L^\alpha = 3c_R^\alpha$ driving force, and no voltage) with the difference that the filter radius was larger and that we used access regions of size $H_B = R_B = 20$ Å. For this reason, we found a different diffusion coefficient ratio ($D_F^{Ca^{2+}}/D_F^{Na^+} \approx 0.125$ compared to 0.5 in the previous case) that reproduced the flux ratio of the dynamical simulation. This ratio is very similar to that found by Gillespie [29].

4.2.1. The effect of voltage

The first AMFE experiment we consider is that published in Fig. 1B of the paper by Gillespie et al. [30]: $CaCl_2$ is added to the luminal side to a 100 mM NaCl background at different voltages. This figure is replotted in Fig. 5A and shows both the experimental data and the curves given be the NP + DFT theory of Gillespie [29] for voltages 10, 20, and 30 mV. Fig. 5B shows the curves computed from the NP + LEMC method for voltages −20, 0, 10, 20, and 30 mV.

The qualitative agreement between the NP + LEMC and experimental data is apparent. The anomalous behavior of the current vs. Ca^{2+} concentration curve is present and the behavior as a function of voltage is similar. Currents increase with increasing voltage, as expected. The absolute value of the current does not agree because we did not fit $D_F^{Na^+}$ to experimental data; we just used the value reported by Gillespie, which is a quite different model. Most importantly, Gillespie used more acidic amino acids in his model that attracted more cations into the channel including the vestibules; this explains the larger current.

Fig. 5B includes results for voltages 0 and −20 mV. AMFE vanishes at these voltages. This can be explained by analyzing Fig. 6, where the electrical currents carried by Ca^{2+} and Na^+ (and their sum) are shown as functions of Ca^{2+} concentration for voltages 20 mV (top panel) and −20 mV (bottom panel). In both cases, the absolute value of the Na^+-current decreases as the Ca^{2+} concentration is increased because Ca^{2+} gradually squeezes Na^+ out of the selectivity filter (see Fig. 4B). The behavior of Ca^{2+}-current, on the other hand, is drastically different. At positive voltage, the Ca^{2+}-current has the same sign as Na^+-current has and it gradually increases, producing a typical AMFE-behavior (similar to Fig. 4A). At negative voltage, however, the Ca^{2+}-current has the opposite sign and it remains small. The explanation is that voltage works against the concentration difference of Ca^{2+} in this case.

Further insight can be gained from the concentration profiles plotted for the different ions in Fig. 7 for $c_L^{Ca^{2+}} = 10^{-3}$ M, and voltages ±20 mV. The cation profiles are different for positive and negative voltages. For −20 mV, Ca^{2+} concentration is depleted on the right hand side in the access region at the positive electrode (see the inset of Fig. 7B; note the logarithmic scale of the inset). This depletion extends into the channel (see the main panel of Fig. 7B). The mechanism behind this effect is complex: it involves all the functions appearing in the NP equation. Basically, because the total driving force (chemical plus electrical potential gradients) is smaller for negative voltage, the flux is smaller. On the right-hand side, this implies decreasing Ca^{2+} concentration.

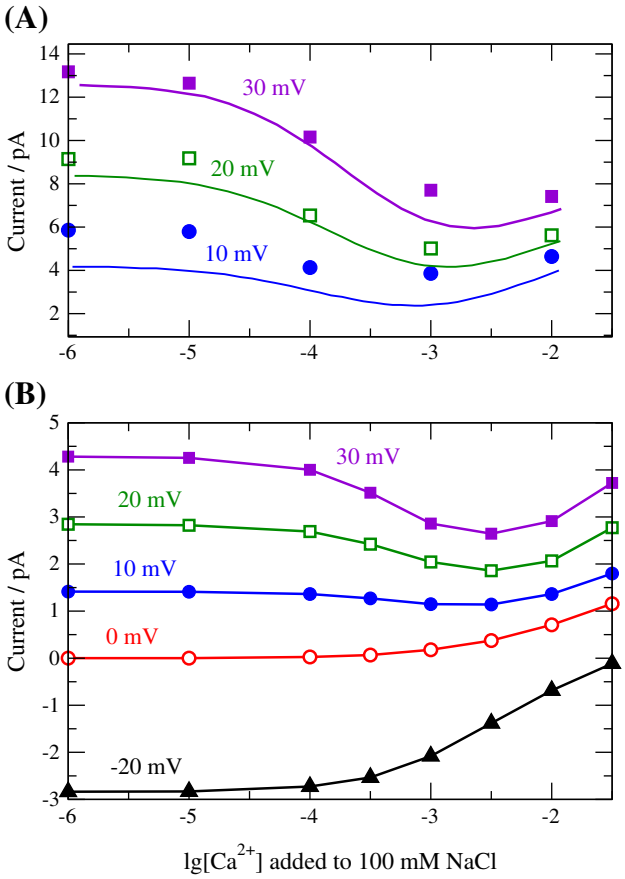

Fig. 5. The added $CaCl_2$ experiment considered by Gillespie et al. [30]. $CaCl_2$ is added to a constant background of 100 mM NaCl to the left hand side of the membrane at different voltages (ground is on the right). Ca^{2+} concentration is micromolar on the right side. The dimensions of the access and bulk regions are 20 and 10 Å, respectively. The resolution of the grid is 2 × 2 Å. Panel (A) replots the results of Fig. 1B of Ref. [30]. Symbols are experiments, while lines are results of NP + DFT calculations. Panel (B) shows the results of our NP + LEMC calculations.

At the same time, Na^+ concentration increases in the selectivity filter, because Na^+ ions are needed there to balance the charge of the oxygen ions (see the main panel of Fig. 7A). Outside the membrane, in the double layer region, Na^+ shows the opposite behavior of Ca^{2+}. For the negative voltage, Na^+ concentration increases in the double layer at the membrane on the right hand side, while, at the same time, Cl^- concentration decreases compared to the positive voltage (see the inset of Fig. 7A). The double layers on the two sides of the membrane are formed to produce an electric field denoted by $\Phi^{ion}(\mathbf{r})$ (see Appendix A for more details). The sum of the applied electric potential and that produced by the ions is the total electrical potential shown in Fig. 7C.

The ionic concentration profiles are formed in the NP + LEMC system in a way that the electrical potential of the ions counteracts the applied field. In Fig. 7, two kinds of double layers can be observed. The dominant ones contain excess of cations forming positive diffuse layers to balance the negative charge of the channel. The negative channel produces the electrical potential well around $z = 0$ Å, while the positive double layers counteract the effect of the channel and bring the level of the potential up to zero.

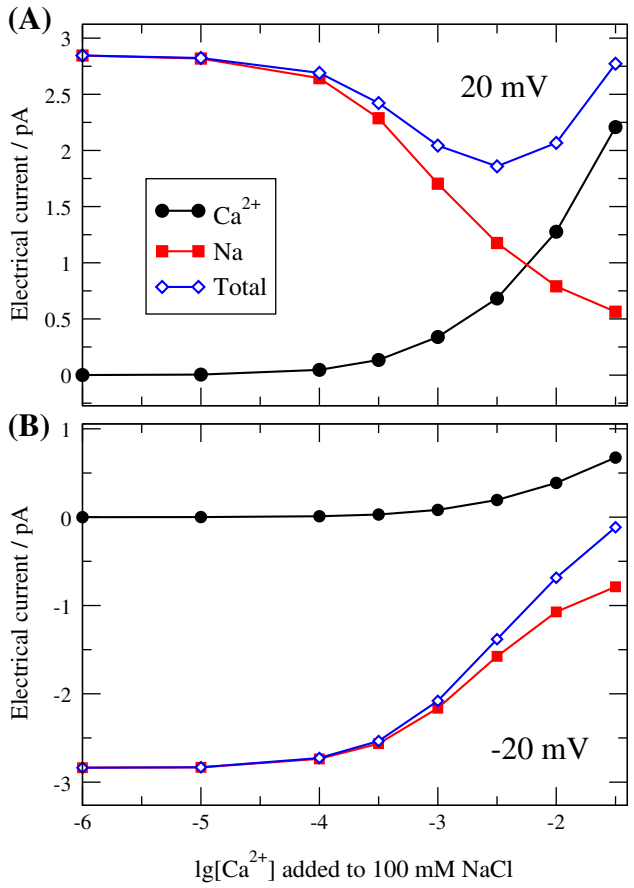

Fig. 6. Electrical currents for the situation depicted in Fig. 5. Currents carried by the different ions (and their sum) are plotted for voltages (A) 20 mV and (B) −20 mV.

The secondary double layers appear because of the applied voltage. For $\Delta\Phi = -20$ mV, for example, the applied electrical potential is monotonically increasing. To counteract this potential and to make the potential profile close to horizontal in the right access region (see Fig. 7C), excess positive charge is needed in the right-side double layer (see Fig. 7A). Similarly, to decrease the potential in the left-side access region, excess negative charge is needed in the left-side double layer.

4.2.2. The effect of NaCl concentration

In the previous experiment, the concentration of the monovalent salt was kept fixed and the voltage was changed. Now, let us consider the opposite: NaCl concentration is changed at constant voltage $\Delta\Phi = 20$ mV. The results are shown in Fig. 8B. The top panel replots the results of Fig. 4 of the paper of Gillespie et al. [30].

The qualitative agreement is again found:

1. Currents are larger for larger NaCl concentrations because more Na^+ ions enter the pore in this case.
2. The current vs. $c_L^{Ca^{2+}}$ curve declines at larger Ca^{2+} concentrations when Na^+ concentration is larger. This is because the ability of Ca^{2+} to compete for the pore with Na^+ depends on the concentration of the other competing ion [25,30]. This can be straightforwardly explained with the energetics behind this selectivity as we did in previous papers [27,29].

5. Summary

We have developed an accessible MC method that couples statistical probabilities of individual ionic configurations to a transport equation. The former establishes a relation between the electrochemical potential and the concentration, while the latter establishes a closure between them and also computes flux density. The advantage of the method is that it treats statistical mechanics in an "exact" manner, meaning that simulations do not contain "built-in" approximations as theories do; they are just subjects of system-size errors and statistical noise. An additional advantage is that electrostatics is treated correctly in every configuration through Coulomb's law and that Dirichlet BCs at the boundary of the system are satisfied if the access regions are large enough (see Appendix A).

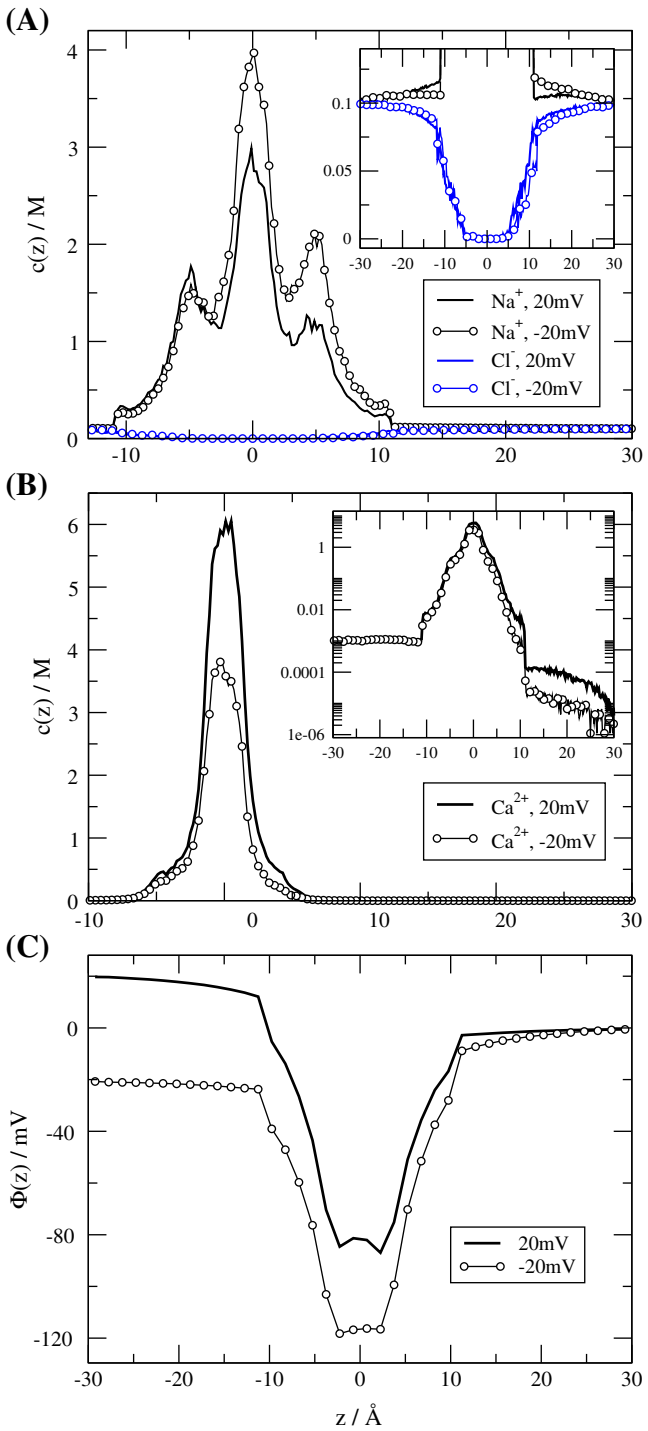

Fig. 7. Profiles for the case depicted in Fig. 5 for $c_L^{Ca^{2+}} = 1$ mM at the two indicated voltages. Panel (A) shows Na^+ and Cl^- concentration profiles (the inset magnifies the small concentration regime), panel (B) shows the Ca^{2+} concentration profiles (the inset uses logarithmic scale for the ordinate), while panel (C) shows the electrical potential profiles.

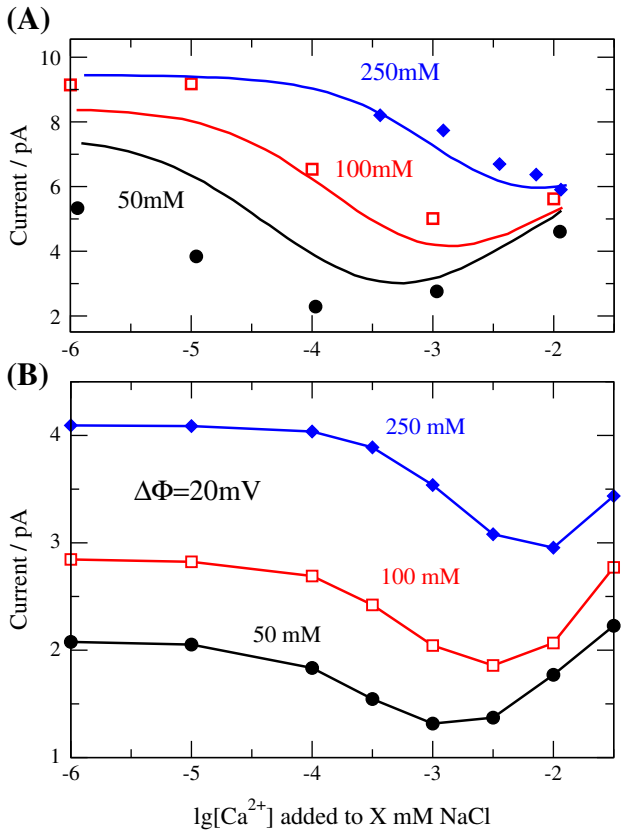

Fig. 8. The added $CaCl_2$ experiment considered by Gillespie et al. [30]. $CaCl_2$ is added to a background of NaCl at the indicated concentration to the left hand side of the membrane at 20 mV voltage (ground is on the right). For other details, see the caption of Fig. 5. Panel (A) replots the results of Fig. 4 of Ref. [30]. Symbols are experiments, while lines are results of NP + DFT calculations. Panel (B) shows the results of our NP + LEMC calculations.

The disadvantage of the method is that it uses the approximation of the NP equation to describe transport, which requires a priori knowledge of the diffusion coefficient. Direct dynamical simulation techniques can replace the NP equation, avoiding the use of this adjustable parameter, but at the cost of considerably larger computational time [41].

Acknowledgment

The Appendix was inspired by the insightful discussions with Bob Eisenberg, whose role in the development of the authors in the research on ion channels and electrodiffusion is gratefully acknowledged. We acknowledge the financial support of the Hungarian State and the European Union under the TAMOP-4.2.2.A-11/1/KONV-2012-0071 and TAMOP-4.2.2/B-10/1-2010-0025. The support of the Hungarian National Research Fund (OTKA K75132) is acknowledged.

Appendix A. Imposing Dirichlet boundary conditions

Treating electrostatics and imposing fixed-voltage BCs (Dirichlet) are crucial aspects of our procedure and they deserve a detailed discussion. We must clearly distinguish between imposing BCs for individual configurations during the simulation and for the averaged profiles.

For a given configuration of the simulation, we have a number of charges in the middle of an empty Universe in a small finite simulation cell. In such a case, BCs are set at infinity and Coulomb's law is applied to compute the energy, a usual way to compute electrostatic energy in simulations of electrolytic systems.

There are two kinds of charges in the system. There are point charges at the centers of the ions

$$\rho(\mathbf{r}) = \sum_k q_k \delta(\mathbf{r}-\mathbf{r}_k), \tag{A.1}$$

where q_k and $\mathbf{r}_k$ are the charge and the position of the kth ion, respectively. There is also a polarization charge, $\sigma^{\mathrm{fix}}(\mathbf{s})$, on the boundary of the solution domain, $\mathcal{B}$, obtained from solving Laplace's equation (Eq. (7)) with the prescribed Dirichlet BCs. Let us denote the part of surface $\mathcal{B}$ on the left and right hand sides with $\mathcal{B}_{\mathrm{L}}$ and $\mathcal{B}_{\mathrm{R}}$, respectively. The BC then can be written as

$$\begin{aligned} \Phi^{\mathrm{appl}}(\mathbf{s}) &= \Phi_{\mathrm{L}} \quad \text{if } \mathbf{s}\in\mathcal{B}_{\mathrm{L}} \\ \Phi^{\mathrm{appl}}(\mathbf{s}) &= \Phi_{\mathrm{R}} \quad \text{if } \mathbf{s}\in\mathcal{B}_{\mathrm{R}}, \end{aligned} \tag{A.2}$$

or we can just denote the potential on $\mathcal{B}$ with $\Phi^{\mathrm{BC}}(\mathbf{s})$ and write

$$\Phi^{\mathrm{BC}}(\mathbf{s}) = \Phi^{\mathrm{appl}}(\mathbf{s}) \tag{A.3}$$

for $\mathbf{s}\in\mathcal{B}$. The polarization charge produces this applied potential everywhere in the domain:

$$\Phi^{\mathrm{appl}}(\mathbf{r}) = \frac{1}{4\pi\epsilon_0}\int_{\mathcal{B}} \frac{\sigma^{\mathrm{fix}}(\mathbf{s}')}{|\mathbf{r}-\mathbf{s}'|} da'. \tag{A.4}$$

If we write up this potential for $\mathcal{B}$, we obtain

$$\Phi^{\mathrm{BC}}(\mathbf{s}) = \frac{1}{4\pi\epsilon_0}\int_{\mathcal{B}} \frac{\sigma^{\mathrm{fix}}(\mathbf{s}')}{|\mathbf{s}-\mathbf{s}'|} da' \tag{A.5}$$

for $\mathbf{s}\in\mathcal{B}$. Thus, we obtain an integral equation for $\sigma^{\mathrm{fix}}(\mathbf{s})$ that can be solved with the ICC method [20,51,67,68]. This polarization charge is also represented as a collection of point charges in this numerical framework, but this is irrelevant for this discussion. The superscript "fix" is used in $\sigma^{\mathrm{fix}}(\mathbf{s})$ because this charge is computed once at the beginning of the simulation and fixed.

In every configuration during the simulation, the electrical potential in the simulation domain is the sum of the potentials produced by the ions and the applied potential:

$$\Phi(\mathbf{r}) = \Phi^{\mathrm{ion}}(\mathbf{r}) + \Phi^{\mathrm{appl}}(\mathbf{r}), \tag{A.6}$$

where

$$\Phi^{\mathrm{ion}}(\mathbf{r}) = \frac{1}{4\pi\epsilon_0\epsilon}\sum_k \frac{q_k}{|\mathbf{r}-\mathbf{r}_k|}. \tag{A.7}$$

How does the NP + LEMC procedure ensure that the Dirichlet BC is satisfied on $\mathcal{B}$? The answer is that it ensures it only on average. This means that the ensemble average of the electrical potential is equal to the prescribed potential:

$$\Phi^{\mathrm{BC}}(\mathbf{s}) = \langle\Phi(\mathbf{s})\rangle = \left\langle\Phi^{\mathrm{ion}}(\mathbf{s})\right\rangle + \Phi^{\mathrm{appl}}(\mathbf{s}) \tag{A.8}$$

for $\mathbf{s}\in\mathcal{B}$ (the brackets denote ensemble average over the configurations sampled in the LEMC simulations). From Eqs. (A.3) and (A.8) we obtain

$$0 = \left\langle\Phi^{\mathrm{ion}}(\mathbf{s})\right\rangle \tag{A.9}$$

for $\mathbf{s}\in\mathcal{B}$. There are four important aspects of the NP + LEMC technique that make this possible.

1. The procedure ensures that the prescribed electrochemical potentials (μ_L^α and μ_R^α, see Eq. (4)) are recovered on $\mathcal{B}$.
2. The functions appearing in the solution of the NP + LEMC system ($\mu^\alpha(\mathbf{r})$, $\mu_c^\alpha(\mathbf{r})$, and $\Phi(\mathbf{r})$) are continuous. The electrochemical potential, moreover, changes smoothly in the transport region between the values on $\mathcal{B}$.
3. In the bulk region and at the boundary, we simulate bulk electrolytes with the prescribed compositions as if they were at zero external potential. This can be seen by considering the acceptance probability of the ion-insertion (Eq. (5)). The term $\Delta U^\alpha(\mathbf{r})-\mu^\alpha(\mathbf{r})$ appears in this formula. The electrostatic energy of the inserted ion, however, contains the interaction with the ions and with the applied field:

$$\Delta U^\alpha(\mathbf{r}) = q^\alpha \Phi^{\text{ion}}(\mathbf{r}) + q^\alpha \Phi^{\text{appl}}(\mathbf{r}). \tag{A.10}$$

   The electrochemical potential can also be split into the chemical and the electrical terms (see Eq. (1)):

$$\mu^\alpha(\mathbf{r}) = \langle \mu_c^\alpha(\mathbf{r}) \rangle + q^\alpha \langle \Phi^\alpha(\mathbf{r}) \rangle. \tag{A.11}$$

   Because the electrical potential can be computed in the simulation as an ensemble average (using a test charge for sampling), the chemical potential, $\mu_c^\alpha(\mathbf{r})$, can also be written as an ensemble average. The electrical potentials in the bulk regions and at $\mathcal{B}$ cancel as soon as Eq. (A.8) holds. In this case, the LEMC simulations look like as if they were performed for bulk electrolytes in the absence of an applied field.
4. This last condition is fulfilled if the access regions are large enough. Ions accumulate in the vicinity of the channel near the membrane and form double layers. The access regions must be large enough to accommodate these double layers, especially the diffuse layers. If $\mathcal{B}$ is far enough from the channel region, where charge imbalance occurs, bulk electrolytes are formed in the access regions and at the boundaries of them.

It is important to emphasize that the BC is satisfied not only by electrostatic methods, but via the whole iteration procedure of the NP + LEMC method involving statistical mechanical calculations. From this point of view, our approach is not different from the NP + DFT method of Gillespie et al. [13,14] or the PNP theory [5,69–74] (which is the Poisson–Boltzmann equation coupled to the NP equation). The difference is that the system can be solved accurately in the case of theories (an additional loop is built into the calculations to satisfy Poisson's equation), while in the case of simulations we are restricted by finite system size effects and statistical errors. Fulfillment of the Dirichlet BC, therefore, is an output of the NP + LEMC calculation. Our solution is an approximation to the accurate solution.

This does not mean that our electrostatics is incorrect. Because Coulomb's law is used for individual configurations, electrostatics must be correct for the ensemble average too. The approximation lies in the possibility that $\langle \Phi^\alpha(\mathbf{s}) \rangle$ is not perfectly equal to $\Phi^{\text{BC}}(\mathbf{s})$ on $\mathcal{B}$.

In order to ensure perfect agreement (within numerical errors) between $\langle \Phi^\alpha(\mathbf{s}) \rangle$ and $\Phi^{\text{BC}}(\mathbf{s})$ on $\mathcal{B}$, we should perform the LEMC simulations in a way that the Dirichlet BCs are fulfilled for every individual ion configuration. This requires solving Poisson's equation with the prescribed Dirichlet BCs "on the fly". This approach was used in BD [75,76] and Transport Monte Carlo [77] simulations. A Poisson solver, however, is also a numerical procedure subject to numerical errors. It can also be time consuming compared to just using Coulomb's law.

Another possibility is using the ICC method [20,51,67,68] to compute the induced charges on $\mathcal{B}$. For this, Eq. (A.5) must be rewritten with the ionic potential included:

$$\Phi^{\text{BC}}(\mathbf{s}) = \Phi^{\text{ion}}(\mathbf{s}) + \frac{1}{4\pi\epsilon_0}\int_{\mathcal{B}} \frac{\sigma^{\text{tot}}(\mathbf{s}')}{|\mathbf{s}-\mathbf{s}'|} da', \tag{A.12}$$

which is an integral equation for the polarization charge $\sigma^{\text{tot}}(\mathbf{s})$ that can be solved with ICC. The total polarization charge now includes the fixed component and a fluctuating component, $\sigma^{\text{fluct}}(\mathbf{s})$, that is different for every configuration of ions, $\{\mathbf{r}_k\}$:

$$\sigma^{\text{tot}}(\mathbf{s}) = \sigma^{\text{fix}}(\mathbf{s}) + \sigma^{\text{fluct}}(\mathbf{s}). \tag{A.13}$$

The integral equation then can be rewritten in terms of the fluctuating charge:

$$0 = \Phi^{\text{ion}}(\mathbf{s}) + \frac{1}{4\pi\epsilon_0}\int_{\mathcal{B}} \frac{\sigma^{\text{fluct}}(\mathbf{s}')}{|\mathbf{s}-\mathbf{s}'|} da'. \tag{A.14}$$

This expresses that the fluctuating charge ensures that the Dirichlet BCs are satisfied in every configuration. The ICC method, however, is very time consuming; it usually increases the computational cost with one or two orders of magnitude.

Our present approach avoids applying the Dirichlet BC "on the fly" thus saving a lot of computational time, since we have to compute the induced charges, $\sigma^{\text{fix}}(\mathbf{s})$, only once at the beginning of the calculation.

The two kinds of solutions are not equivalent because they correspond to different Hamiltonians. Which one is closer to an experimental situation is an interesting question. Applying Dirichlet BC "on the fly" means perfect polarizability, meaning that charges can respond to the movement of ions infinitely fast. This is clearly an idealization; in reality, every particle has inertia. This implies that satisfying the BC only on average actually might be a more realistic approach. In a new method by Jadhao et al. [78], the induced charges are actually treated as dynamical variables with assigned masses in an MD scheme.

This is very similar to the classic double layer simulations, where we simulate an electrolyte between two charged walls (electrodes). We can impose fixed potentials on the electrodes "on the fly" with a PDE solver or ICC as described above. We are not aware of such a simulation. The alternative (a relative of the approach used in NP + LEMC) is the constant voltage simulation technique by Kiyohara and Asaka [79,80] that is based on treating voltage as a variable of a thermodynamic ensemble. Then, an MC step is introduced in which a charge transfer occurs between the electrodes. At the end of the simulation, ionic concentration profiles are obtained that produce a potential profile that, in turn, satisfies the prescribed potential difference between the electrodes. The parallels between this approach and the NP + LEMC technique are unmistakable.

Treating electrons and holes in semiconductors [81–83] is similar to treating anions and cations in electrolytes from many points of view. The basic requirement that electrostatics must be correct is the most important parallel. Semiconductor devices, for example, can also be described with the PNP theory with great success. There are, however, very important differences. Electrons and holes can be treated as point charges in a background dielectric, therefore, using the terminology of physical chemistry, they can be considered as ideal solutions. This means that they can be described by the Poisson–Boltzmann theory. Solving Poisson's equation is the dominant problem in the case of semiconductors, which is performed with great precision for finite size systems modeling the various devices prescribing appropriate BC at the boundary of the system.

Electrolytes, however, are far from being ideal solutions [84], especially in the high-density selectivity filter of an ion channel. Mean field theories are not sufficient anymore and sophisticated statistical mechanical methods are necessary to average the microstates. Electrostatics, however, must be correct in this case too. In practice, the problem is seemingly approached from two different directions:

1. In theories using the averaged profiles as variables, solving Poisson's equation is traditionally done with great care. Building statistical mechanical correlations beyond the mean-field level (such as excluded

volume effects and many-body correlations between ions) into the theories, however, is a challenge, which has been taken up by several groups worldwide. The NP + DFT method of Gillespie et al. [13,14] is an example of success, although the method is restricted to one dimension. The task of extending it to three dimensions has been undertaken [85]. The variational approach of Liu and coworkers [15–18] works in three dimensions efficiently dealing with electrostatics and hydrodynamics with considerable effort exerted to handle statistical mechanics.

2. In simulations working with individual configurations, statistical mechanics is treated right traditionally because the method itself is designed for that purpose. Electrostatics is usually treated with Coulomb's law, which ensures that electrostatics is right instantaneously, and, therefore, on average with BCs prescribed at infinity. Prescribing electrostatic BCs on the boundaries of a finite system, however, received less attention because simulations are originally designed for equilibrium systems. With the increasing demand for simulations to model actual experimental situations, however, the requirement to impose electrostatic BCs on the boundary of a finite-size system rose. In this paper, we showed an example how to do it on average. To impose BCs for every configuration is computationally more demanding [75–77]. In future work, we intend to study and compare the two approaches.

References

[1] J. Kärger, Adsorption 9 (2003) 29–35.
[2] E. Csányi, T. Kristóf, G. Lendvay, Journal of Physical Chemistry C 113 (2009) 12225–12235.
[3] E. Csányi, Z. Ható, T. Kristóf, Journal of Molecular Modeling 18 (2012) 2349–2356.
[4] J. Cervera, B. Schiedt, R. Neumann, S. Mafe, P. Ramirez, The Journal of Chemical Physics 124 (2006) 104706.
[5] D. Constantin, Z.S. Siwy, Physical Review E 76 (2007) 041202.
[6] J. Cervera, P. Ramírez, S. Mafe, P. Stroeve, Electrochimica Acta 56 (2011) 4504–4511.
[7] B. Hille, Ion Channels of Excitable Membranes, 3rd ed. Sinauer Associates, Sunderland, 2001.
[8] D.P. Tieleman, P.C. Biggin, G.R. Smith, M.S.P. Sansom, Quarterly Reviews of Biophysics 34 (2001) 473–561.
[9] M.R. Powell, L. Cleary, M. Davenport, K.J. Shea, Z.S. Siwy, Nature Nanotechnology 6 (2011) 798–802.
[10] W.A. Sather, E.W. McCleskey, Annual Review of Physiology 65 (2003) 133–159.
[11] W. Nonner, D.P. Chen, B. Eisenberg, Biophysical Journal 74 (1998) 2327–2334.
[12] W. Nonner, L. Catacuzzeno, B. Eisenberg, Biophysical Journal 79 (2000) 1976–1992.
[13] D. Gillespie, W. Nonner, R.S. Eisenberg, Journal of Physics: Condensed Matter 14 (2002) 12129–12145.
[14] D. Gillespie, W. Nonner, R.S. Eisenberg, Physical Review E 68 (2003) 031503.
[15] B. Eisenberg, Y.-K. Hyon, C. Liu, The Journal of Chemical Physics 133 (2010) 104104.
[16] Y. Hyon, B. Eisenberg, C. Liu, Communications in Mathematical Sciences 9 (2011) 459–475.
[17] T.-L. Horng, T.-C. Lin, C. Liu, B. Eisenberg, The Journal of Physical Chemistry. B 116 (2012) 11422–11441.
[18] Y. Hyon, J.E. Fonseca, B. Eisenberg, C. Liu, Discrete and Continuous Dynamical Systems – Series B 17 (2012) 2725–2743.
[19] G. Rutkai, D. Boda, T. Kristóf, Journal of Physical Chemistry Letters 1 (2010) 2179–2184.
[20] D. Boda, M. Valiskó, B. Eisenberg, W. Nonner, D. Henderson, D. Gillespie, The Journal of Chemical Physics 125 (2006) 034901.
[21] D. Boda, M. Valiskó, B. Eisenberg, W. Nonner, D. Henderson, D. Gillespie, Physical Review Letters 98 (2007) 168102.
[22] D. Boda, W. Nonner, M. Valiskó, D. Henderson, B. Eisenberg, D. Gillespie, Biophysical Journal 93 (2007) 1960–1980.
[23] D. Boda, W. Nonner, D. Henderson, B. Eisenberg, D.D. Gillespie, Biophysical Journal 94 (2008) 3486–3496.
[24] D. Boda, M. Valiskó, D. Henderson, D. Gillespie, B. Eisenberg, M.K. Gilson, Biophysical Journal 96 (2009) 1293–1306.
[25] D. Boda, M. Valiskó, D. Henderson, B. Eisenberg, D. Gillespie, W. Nonner, The Journal of General Physiology 133 (2009) 497–509.
[26] A. Malasics, D. Gillespie, W. Nonner, D. Henderson, B. Eisenberg, D. Boda, Biochimica et Biophysica Acta - Biomembranes 1788 (2009) 2471–2480.
[27] D. Boda, J. Giri, D. Henderson, B. Eisenberg, D. Gillespie, The Journal of Chemical Physics 134 (2011) 055102.
[28] D. Gillespie, L. Xu, Y. Wang, G. Meissner, The Journal of Physical Chemistry. B 109 (2005) 15598–15610.
[29] D. Gillespie, Biophysical Journal 94 (2008) 1169–1184.
[30] D. Gillespie, J. Giri, M. Fill, Biophysical Journal 97 (2009) 2212–2221.
[31] W. Almers, E.W. McCleskey, P.T. Palade, The Journal of Physiology 353 (1984) 565–583.
[32] W. Almers, E.W. McCleskey, The Journal of Physiology 353 (1984) 585–608.
[33] M.P. Allen, D.J. Tildesley, Computer Simulation of Liquids, New York, Oxford, 1987.
[34] D. Frenkel, B. Smit, Understanding Molecular Simulations, Academic Press, San Diego, 1996.
[35] R.J. Sadus, Molecular Simulation of Fluids; Theory, Algorithms, and Object-Orientation, Elsevier, Amsterdam, 1999.
[36] G. Rutkai, T. Kristóf, The Journal of Chemical Physics 132 (2010) 124101.
[37] G.S. Heffelfinger, F. van Swol, The Journal of Chemical Physics 100 (1994) 7548.
[38] M. Lísal, J.K. Brennan, W.R. Smith, F.R. Siperstein, The Journal of Chemical Physics 121 (2004) 4901.
[39] D. Boda, D. Gillespie, Journal of Chemical Theory and Computation 8 (2012) 824–829.
[40] S. Kjelstrup, D. Bedeaux, I. Inzoli, J.-M. Simon, Energy 33 (2008) 1185–1196.
[41] Z. Ható, D. Boda, T. Kristóf, The Journal of Chemical Physics 137 (2012) 054109.
[42] D. Gillespie, D. Boda, Biophysical Journal 95 (2008) 2658–2672.
[43] M. Malasics, D. Boda, M. Valiskó, D. Henderson, D. Gillespie, Biochimica et Biophysica Acta - Biomembranes 1798 (2010) 2013–2021.
[44] E. Csányi, D. Boda, D. Gillespie, T. Kristóf, Biochimica et Biophysica Acta - Biomembranes 1818 (2012) 592–600.
[45] J. Giri, J. Fonseca, D. Boda, D. Henderson, B. Eisenberg, Physical Biology 8 (2011) 026004.
[46] D. Boda, D.D. Busath, D. Henderson, S. Sokołowski, The Journal of Physical Chemistry. B 104 (2000) 8903–8910.
[47] D. Boda, D. Henderson, D.D. Busath, The Journal of Physical Chemistry. B 105 (2001) 11574–11577.
[48] D. Boda, D. Henderson, D.D. Busath, Molecular Physics 100 (2002) 2361–2368.
[49] D. Boda, D.D. Busath, B. Eisenberg, D. Henderson, W. Nonner, Physical Chemistry Chemical Physics 4 (2002) 5154–5160.
[50] J. Vincze, M. Valiskó, D. Boda, The Journal of Chemical Physics 133 (2010) 154507.
[51] D. Boda, D. Gillespie, W. Nonner, D. Henderson, B. Eisenberg, Physical Review E 69 (2004) 046702.
[52] Z.X. Tang, L.E. Scriven, H.T. Davis, The Journal of Chemical Physics 97 (1992) 494–503.
[53] Z.X. Tang, L.E. Scriven, H.T. Davis, The Journal of Chemical Physics 100 (1994) 4527–4530.
[54] L.R. Zhang, H.T. Davis, H.S. White, The Journal of Chemical Physics 98 (1993) 5793–5799.
[55] T. Kristóf, D. Boda, I. Szalai, D. Henderson, The Journal of Chemical Physics 113 (2000) 7488–7491.
[56] D. Boda, D. Henderson, A. Patrykiejew, S. Sokołowski, The Journal of Chemical Physics 113 (2000) 802–806.
[57] D. Boda, D. Henderson, The Journal of Chemical Physics 112 (2000) 8934–8938.
[58] W. Nonner, D. Gillespie, D. Henderson, B. Eisenberg, The Journal of Physical Chemistry. B 105 (2001) 6427–6436.
[59] A. Malasics, D. Gillespie, D. Boda, The Journal of Chemical Physics 128 (2008) 124102.
[60] A. Malasics, D. Boda, The Journal of Chemical Physics 132 (2010) 244103.
[61] B. Widom, The Journal of Chemical Physics 39 (1963) 2808–2812.
[62] B. Widom, Journal of Statistical Physics 19 (1978) 563–574.
[63] J.L. Jackson, L.S. Klein, Physics of Fluids 7 (1964) 228–231.
[64] T.L. Beck, M.E. Paulaitis, L.R. Pratt, The Potential Distribution Theorem and Models of Molecular Solutions, Cambridge University Press, Cambridge, 2006.
[65] K. Binder, Monte Carlo Methods in Statistical Physics, Springer, Heidelberg, 1979.
[66] H.E.A. Huitema, J.P. van der Eerden, The Journal of Chemical Physics 110 (1999) 3267–3274.
[67] A. Peyser, W. Nonner, Physical Review E 86 (2012) 011910.
[68] A. Peyser, W. Nonner, European Biophysics Journal 41 (2012) 705–721.
[69] D. Chen, J. Lear, B. Eisenberg, Biophysical Journal 72 (1997) 97–116.
[70] W. Nonner, B. Eisenberg, Biophysical Journal 75 (1998) 1287–1305.
[71] B. Corry, S. Kuyucak, S.H. Chung, Biophysical Journal 78 (2000) 2364–2381.
[72] Z. Schuss, B. Nadler, R.S. Eisenberg, Physical Review E 6403 (2001) 036116.
[73] S.Y. Noskov, W. Im, B. Roux, Biophysical Journal 87 (2004) 2299–2309.
[74] P. Graf, M.G. Kurnikova, R.D. Coalson, A. Nitzan, The Journal of Physical Chemistry. B 108 (2004) 2006–2015.
[75] S. Aboud, D. Marreiro, M. Saraniti, R. Eisenberg, Journal of Computational Electronics 3 (2004) 117–133.
[76] M. Saraniti, S. Aboud, R. Eisenberg, Reviews in computational chemistry 22 (2005) 229–294.
[77] T.A. van der Straaten, G. Kathawala, R.S. Eisenberg, U. Ravaioli, Molecular Simulation 31 (2004) 151–171.
[78] V. Jadhao, F.J. Solis, M.O. de la Cruz, Physical Review Letters 109 (2012) 223905.
[79] K. Kiyohara, K. Asaka, The Journal of Chemical Physics 126 (2007) 214704.
[80] K. Kiyohara, K. Asaka, Journal of Physical Chemistry C 111 (2007) 15903–15909.
[81] S. Selberherr, Analysis and Simulation of Semiconductor Devices, Springer-Verlag, New York, 1984.
[82] C. Jacoboni, P. Lugli, The Monte Carlo Method for Semiconductor Device Simulation, Springer-Verlag, New York, 1989.
[83] B. Eisenberg, Living transistors: a physicist's view of ion channels. version 2, http://arxiv.org/q-bio.BM:arXiv:q-bio/0506016v22005.
[84] B. Eisenberg, Chemical Physics Letters 511 (2011) 1–6.
[85] M.G. Knepley, D.A. Karpeev, S. Davidovits, R.S. Eisenberg, D. Gillespie, The Journal of Chemical Physics 132 (2010) 124101.